Articles in PresS. J Neurophysiol (November 26, 2014). doi:10.1152/jn.00629.2014

Microchip amplifier for *in vitro, in vivo,* and automated whole-cell patch-clamp recording

Reid R. Harrison[1]

Ilya Kolb[2]

Suhasa B. Kodandaramaiah[3, 4]

Alexander A. Chubykin[5]

Aimei Yang[3]

Mark F. Bear[6]

Edward S. Boyden [3,4]*

Craig R. Forest [7]*

*equal contribution

RRH designed and fabricated the chip.

IK, SBK, AAC, AY performed validation experiments.

MFB, ESB, CRF directed the study.

RRH, IK, SBK, AAC, ESB, CRF wrote the paper.

Running Head:

Miniaturized patch-clamp amplifier

Affiliations:

[1]Intan Technologies, Los Angeles, California

[2]Wallace H. Coulter Department of Biomedical Engineering, Georgia Institute of Technology, Atlanta, Georgia

[3]Media Lab, Massachusetts Institute of Technology, Cambridge, Massachusetts

[4]McGovern Institute, Massachusetts Institute of Technology, Cambridge, Massachusetts

[5]The Department of Biological Sciences, Purdue University, West Lafayette, Indiana

[6]Howard Hughes Medical Institute, The Picower Institute for Learning and Memory, Department of Brain and Cognitive Sciences, Massachusetts Institute of Technology, Cambridge, Massachusetts

[7]George W. Woodruff School of Mechanical Engineering, Georgia Institute of Technology, Atlanta, Georgia

Address for correspondence:

Reid Harrison, Ph.D.
Intan Technologies, LLC
8726 S. Sepulveda Blvd., Suite D2121 | Los Angeles, CA 90045 USA
Ph: +1.424.277.3790 (direct)
Fax: +1.720.834.3750
Email: rharrison@intantech.com

Abstract

Patch-clamping is a gold-standard electrophysiology technique that has the temporal resolution and signal to noise ratio capable of reporting single ion channel currents, as well as electrical activity of excitable single cells. Despite its usefulness and decades of development, the amplifiers required for patch-clamping are expensive and bulky. This has limited the scalability and throughput of patch-clamping for single ion channel and single-cell analyses. In this work, we have developed a custom patch-clamp amplifier microchip that can be fabricated using standard commercial silicon processes capable of performing both voltage and current clamp measurements. A key innovation is the use of nonlinear feedback elements in the voltage clamp amplifier circuit to convert measured currents into logarithmically encoded voltages thereby eliminating the need for large high-valued resistors - a factor that has limited previous attempts at integration. Benchtop characterization of the chip shows low levels of current noise (1.1 pA rms over 5 kHz) during voltage-clamp measurements and low levels of voltage noise (8.2 μV rms over 10 kHz) during current-clamp measurements. We demonstrate the ability of the chip to perform both current and voltage clamp measurement *in vitro* in HEK293FT cells and cultured neurons. We also demonstrate its ability to perform *in vivo* recordings as part of a robotic patch-clamping system. The performance of the patch-clamp amplifier microchip compares favorably with much larger commercial instrumentation, enabling bench-top commoditization, miniaturization and scalable patch-clamp instrumentation.

Keywords: electrophysiology, patch-clamp, electronics, in-vivo, in-vitro

Introduction

Patch-clamp electrophysiology has been a central tool of neuroscience and pharmaceutical research since its advent in the late 1970s (Neher and Sakmann, 1976). The technique of patch-clamping utilizes glass micropipettes and sensitive analog electronics to monitor the synaptic currents and intracellular voltages of individual excitable cells. This is accomplished using micromanipulators to guide a fine micropipette tip into contact with a cell's membrane to create a tight physical connection (or "gigaseal") between the tip of the pipette and the cell membrane. If necessary, it is possible to apply suction pulses to 'break-in' through the

membrane and gain access to the cell cytoplasm, creating a “whole-cell” configuration (Hamill et al., 1981; Margrie et al., 2002; Molleman, 2002). Ultra-low noise microelectrode amplifiers are then used to monitor and manipulate the cell’s picoamp-scale current signals and millivolt-scale voltage signals. Feedback circuitry within the patch-clamp amplifier can enable the user to hold the cell’s membrane voltage constant while monitoring the ionic current flux in and out of the cell using a technique known as voltage clamp (Safronov and Vogel, 1999). In neuroscience, the voltage clamp technique has been used extensively to characterize basic biophysical properties of neurons (Hodgkin and Huxley, 1952). Alternatively, the user may perform a “current clamp” experiment – injecting current into the cell to observe voltage fluctuations such as action potentials (APs) and low-amplitude subthreshold events.

Here we report on the development and testing of a custom patch-clamp microchip, or “PatchChip”, that performs the functions of a traditional patch-clamp electrophysiology rig, but is much smaller, lighter, and requires lower power. Whereas a traditional patch-clamp amplifier consists of a head stage connected to a rack-mounted amplifier/acquisition unit with a cable carrying sensitive analog signals, PatchChip incorporates all amplifier functions in one small device and requires only a small number of additional components on the head stage circuit board to produce a robust digital signal that interfaces to a host computer via a USB adapter. All amplifier control is performed through a software graphical user interface (GUI).

Materials and Methods

Voltage clamp design

A simplified circuit schematic of a traditional patch-clamp amplifier for whole-cell voltage clamp experiments is shown in Fig. 1 (Molleman, 2002; Sakmann and Neher, 2009). In voltage clamp mode, an operational amplifier (“op amp”) is used in a feedback loop to hold or “clamp” the cell membrane potential to a user-specified value V_{clamp}. An op amp with field effect transistor (FET) inputs is used in these applications to ensure that current flowing into the input terminals will be less than a picoamp in magnitude (Sigworth, 1995; Sakmann and Neher, 2009). Thus, the whole-cell current I_{cell}, resulting from the sum of all ion channel activity in the cell membrane, is forced through one of the feedback resistors R_{Fn}, converting the current into a linearly

proportional voltage that is digitized by an analog-to-digital converter (ADC) and sent to a computer for analysis and storage. The properties of various types of ion channels are studied by methodically sweeping V_{clamp} over a range of roughly ±100 mV and monitoring the magnitude and time course of the resulting whole-cell currents. Additional circuits not shown in Fig. 1 compensate for the resistance R_P and capacitance C_P of the pipette.

Since the resulting output voltage (V_{out}) is equal to $I_{cell}R_F$ (after the known voltage V_{clamp} has been subtracted), a value of R_F must be selected that scales tiny picoamp or nanoamp currents to a convenient voltage for ADCs: millivolts or volts. This requires extremely high-valued resistors in the range of 10 MΩ to 50 GΩ. Since currents can vary widely (e.g. 10-50 pA with a single synapse active; 2-3 nA with many synapses active) a bank of resistors with a broad range of R_F values is required, and the user must select a range that provides good resolution without overloading the ADC. Building circuit boards for measuring picoamp currents is challenging: contamination from a fingerprint or residual solder flux can create parasitic gigaohm-level resistances that short out R_F components; large feedback resistors must be protected from surface oxidation or moisture. Integrating the critical feedback elements on the same chip as the op amp would reduce the size and cost of these circuits.

Recent work has integrated the traditional patch-clamp amplifier shown in Fig. 1 in a 0.5-µm silicon-on-sapphire complementary metal-oxide-semiconductor (CMOS) fabrication process (Laiwalla et al., 2006; Weerakoon et al., 2010; Goldstein et al., 2011). It is difficult to create large-valued resistors on a chip: there are typically only one or two types of resistive material available, so to create higher resistances the only option is to create longer and longer serpentine traces of resistive material. This resistive material is deposited on a thin insulating layer covering the underlying silicon wafer, so larger resistors have larger parasitic capacitances to the chip substrate which can cause stability problems in feedback loops. Limited chip area and undesirable stray capacitances make it difficult to build high quality on-chip resistors in the high MΩ range. Previous research efforts managed to integrate resistors in the range of 10-100 MΩ onto chips, but this is at the low end of feedback resistances used in traditional patch-clamp amplifiers, and the ability to resolve small currents suffered as a result. A current noise floor of 8 pA rms over a 10 kHz bandwidth was reported (Weerakoon et

al., 2010). In comparison, commercial voltage clamp systems have current noise floors more than ten times lower over equivalent bandwidths (Molecular Devices).

To achieve higher sensitivity with a fully integrated patch-clamp amplifier, we designed and simulated a novel voltage clamp circuit architecture that eliminates the need for very large feedback resistors. The circuit, shown in simplified form in Fig. 2A, uses on-chip diode-like circuit elements in the feedback path in place of resistors. Diodes have an exponential *I-V* relationship when they are forward biased; the forward current through the diode (i_D) is an exponential function of the voltage across the diode (v_D):

$$i_D = I_S\left(e^{v_D/(nV_T)} - 1\right) \approx I_S e^{v_D/(nV_T)}$$

for $v_D > 0$, where I_S is a device constant with units of current, n is a constant approximately equal to 1.5, and V_T is the thermal voltage kT/q, which is approximately 26 mV at room temperature. When $v_D < 0$, the diode current approaches I_S, which is far below one picoamp, so we can consider the reverse current to be practically zero. By placing two anti-parallel diode-like devices D_1 and D_2 (actually subthreshold FETs (Vittoz and Fellrath, 1977; Mead, 1989)) in the feedback loop as shown in Fig. 2, we ensure that one of the devices is always on and the other off, depending on the direction of I_{cell}. By placing the diodes in a feedback loop, we invert the exponential current-voltage relationship and produce an output voltage that is a logarithmic function of the measured current I_{cell}:

$$V_{\text{out}} = V_{\text{clamp}} \pm nV_T \ln \frac{|I_{\text{cell}}|}{I_S}$$

where the sign depends on the direction of current. The output voltage encodes a signed, logarithmically compressed measure of cell current. This representation has significant advantages for voltage clamp applications: it allows a wide range of currents (ranging from picoamps to microamps), both positive and negative, to be represented in a limited voltage range that is compatible with an analog-to-digital converter. Relative current changes are encoded as constant voltage steps; the entire range of currents from 1 pA to 1 μA encompasses a voltage range of only 0.54 V. After sampling V_{out} with a standard 16-bit ADC, relative current changes of less than 0.1% will be discernable across this entire range. Cellular currents spanning many orders of magnitudes can be measured without having to switch between different feedback resistors.

The current-voltage relationship of the diode-like elements is affected by ambient temperature: V_T is proportional to temperature and I_S, too, varies with temperature. To address this problem, we integrated an on-chip temperature sensor (Tuthill, 1998) near the diodes (Fig. 2A). A calibration is performed for both diodes to resolve their individual dependence on temperature and correct for it. Their temperature dependence does not vary over time, thus the calibration step only needs to be performed once for each PatchChip device. This calibration is then used to factor out diode temperature dependencies in software. The software also converts the logarithmically-encoded output voltage into a linear measure of current for display and recording, and performs a self-calibration of the voltage clamp circuits upon power-up.

Fig. 2B shows a detailed schematic of the voltage clamp circuit. Transistors M1 and M2 operate in subthreshold mode and act like diodes, producing a current that is an exponential function of V_{out}. For positive values of V_{out}, M1 is active and M2 is off; for negative values of V_{out}, M2 is active and M1 is off. The current mirrors M3-M4 and M5-M6 redirect these currents and produce a feedback current I_F. The op amp drives V_{out} to a value that equalizes I_F and I_{cell}. The feedback capacitor C_F ensures that the feedback loop comprising the op amp and transistors M1-M6 remains stable.

Current clamp design

The majority of patch-clamp experiments use the voltage clamp configuration to hold a membrane potential and measure the resulting currents. However, many experiments require use of the current clamp configuration where a constant current is injected into the cell (though often this current is set to zero) and the resulting intracellular potential is measured. This mode allows neurons to fire action potentials naturally, with magnitudes between 50 and 100 mV. This mode also allows measurement of single millivolt-scale sub-threshold activity.

The circuit components of a current clamp amplifier are: (1) a voltage buffer or amplifier with low input-referred voltage noise that can drive an ADC; and (2) a programmable current source. Most traditional patch-clamp amplifiers use a unity-gain buffer for monitoring intracellular voltages. A noise floor less than 25 μVrms over a bandwidth of 10 kHz is desired for high signal quality.

We designed a DC-coupled current-clamp voltage amplifier using low-noise amplifier circuitry based on principles developed by Harrison and Charles (Harrison and Charles, 2003). A gain of 4 was incorporated to

boost the signal before it is digitized by the ADC. We also designed transistor-based programmable current sources to inject positive or negative currents over a wide range from 5 pA to 128 nA.

In-vitro whole cell patch-clamping in HEK293FT cells

We performed whole cell patch-clamp recordings from HEK293FT (Invitrogen) cells using the PatchChip. The HEK293FT cells were maintained between 10% to 70% confluence in DMEM cell culture medium (Cellgro) and supplemented with 10% fetal Bovine serum (Invitrogen), 1% penicillin/streptomycin (Cellgro) and 1% sodium pyruvate (Biowhitaker). 1-2 days before recording, cells were plated at 5-20% confluence on glass coverslips coated with Matrigel (BD Biosciences). For the recordings, the cells were kept in extracellular solution (Tyrode's solution) consisting of (mM): 125 NaCl, 2 KCl, 3 CaCl2, 1 MgCl2, 10 HEPES, 30 glucose. The pH of tyrode's solution was adjusted to 7.3 using NaOH and the osmolarity was 305 mOsm. Patch pipettes with resistances 4-6 MΩ were pulled from borosilicate glass capillaries (Warner Instruments) using a P97 pipette puller (Sutter Inc). The pipettes were filled with intracellular solution consisting of (in mM)- 135 potassium gluconate (with more added empirically at the end, to bring osmolarity up to ~290 mOsm), 0.1 CaCl2, 0.6 MgCl2, 1 EGTA, 10 HEPES, 4 MgATP, 0.4 Na GTP and 8 NaCl (pH adjusted to 7.2 by addition of KOH) as described previously (Klapoetke et al., 2014).

In-vitro whole cell patch-clamping in cultured neurons

All animal procedures were approved by the Committee on Animal Care at the Massachusetts Institute of Technology. Primary hippocampal neuronal cultures were prepared from E18 mouse embryos as previously described (Chen and Bear, 2007). Hippocampi were dissected in ice-cold dissociation medium and digested for 1 h in 0.01% papain for 1h at 37°C. Neurons were triturated with a siliconized Pasteur pipette, and then were plated onto 12-mm glass coverslips coated with poly-lysine. Culture media consisted of Neurobasal A, 2% B27 supplement, 100 units/mL penicillin, 100 µg/mL streptomycin, 0.5 mM l-glutamine. In a subset of experiments, a sodium channel blocker (1 µM TTX) was added to inhibit action potential generation. Cultures were maintained at 37°C in a humidified incubator gassed with 95% air and 5% CO2. The pipette internal solution for current-clamp recordings contained 20 mM KCl, 100 mM Na-gluconate, 10 mM HEPES, 4 mM

MgATP, 0.3 mM Na2GTP, 7 mM phosphocreatine-Tris, and 0.2% biocytin with pH adjusted to 7.2 and osmolarity adjusted to 300 mOsm; the internal solution for voltage-clamp contained 103 mM Cs-gluconate, 5 mM TEA-Cl, 2.8 mM NaCl, 20 mM HEPES, 0.3 mM Na2GTP, 4 mM MgATP, 10 mM Na2-phosphocreatine, 0.2 mM EGTA, 0.2% biocytin, and 5 mM QX-314-Cl with pH adjusted to 7.2 and osmolarity adjusted to 300 mOsm with sucrose or ddH2O.

In-vivo whole cell patch-clamping

All animal procedures were approved by the Institutional Animal Care and Use Committee at the Georgia Institute of Technology. Methodology to perform automated whole-cell patch-clamp electrophysiology has been previously described (Kodandaramaiah et al., 2012). Briefly, an adult male C57/BL6 mouse, 8 weeks old, was anesthetized using a cocktail of ketamine and xylazine initially at 100 mg kg−1 and 10 mg kg−1, respectively, and redosed at 30–45 min intervals with 10–15% of the initial ketamine dose as needed if the animal was responsive to toe pinch. The subject was affixed in a stereotaxic apparatus (Kopf) and a headplate implant was attached, followed by opening of a craniotomy 1 mm wide above the barrel cortex (centered 0.83 mm posterior and 3.0 mm lateral to bregma) using previously described protocols (Margrie et al., 2002; Kodandaramaiah et al., 2012). Once opened, the craniotomy was superfused with sterile saline throughout the experiment to keep the tissue moist. The anesthetized animal was then headfixed using a custom 3D-printed holder. Pipette solution was the same as in the *in vitro* preparation. Pipette capacitance was compensated in voltage clamp. No bridge balance compensation was performed.

Results

Benchtop testing

We designed and fabricated the PatchChip in a commercially available 0.35-µm silicon CMOS process. We used an “analog friendly” process that allowed for the fabrication of high quality capacitors and resistors in addition to standard transistors that are used to build analog and digital circuits. The 0.35-µm feature size was smaller than the 0.5-µm feature size used by previously published patch-clamp microcircuits (Sigworth, 1995;

Laiwalla et al., 2006; Weerakoon et al., 2010; Goldstein et al., 2011) and offered higher performance due to smaller transistor gate lengths and lower threshold voltages.

Each microfabricated PatchChip (Fig. 3A) is 4.7 mm × 3.0 mm in size and contains more than 20,000 transistors, resistors, and capacitors. The chips were packaged in standard Plastic Leaded Chip Carrier (PLCC) packages to facilitate standard solder assembly onto circuit boards.

A custom printed circuit board (PCB) was designed to connect the PatchChip to supporting circuits including voltage regulators and a 16-bit ADC. The PCB was placed inside a grounded aluminum case to provide Faraday shielding from interference and other sources of noise. A 7/16 x 20 threaded connector or a coaxial connector (pictured in Fig. 3B) was attached to the case to interface with commonly used pipette holders. This complete assembly acted as headstage where the patch pipettes were mounted. Two connectors on the right side of the case provided connection points for interface cables that delivered power and digital signals to and from the PCB. These cables connected to a small USB interface board that allowed the PatchChip to be controlled and monitored by a host computer over a standard USB cable. Digital commands configured the patch-clamp electronics and selected amplifier modes and voltage/current clamp values.

We also developed custom graphical user interface (GUI) software that allowed users to easily control the PatchChip. All software was written in C++ using the open-source Qt libraries (Qt Project Hosting; Oslo, Norway) to allow for cross-platform compilation under Windows, Mac, or Linux operating systems.

The interface software allows users to control and monitor voltage clamp and current clamp experiments. For example, users can apply voltage steps and measure the resulting time-varying currents (in voltage clamp mode), or apply current steps and record the intracellular voltage (in current clamp mode). Measured current or voltage waveforms can be saved to disk and software was developed to load these data files into MATLAB (Mathworks, Natick, MA). Multiple copies of the circuit board were built and used at various labs in different experimental settings, and the software was run on various computers. Both the hardware and software performed robustly in all settings.

The PatchChip is able to resolve voltages down to 8.2 μV and currents as small as 1.1 pA (Table 1). This is an improvement over the previously published chip (Weerakoon et al., 2010; Goldstein et al., 2011) and compares favorably to commercial patch-clamp amplifiers already on the market. For example, the commonly used Axopatch 200B patch-clamp amplifier from Molecular Devices has a current noise floor of 0.65 pA rms in high gain mode or 1.65 pA rms in low gain mode when the bandwidth is set to 5 kHz. This is comparable to our noise floor of 1.1 pA rms across 5 kHz as measured in voltage clamp mode over 100 ms (Fig. 3C). The Axoclamp 900A microelectrode amplifier, also from Molecular Devices, has a voltage noise floor of 23 μVrms across a 10 kHz bandwidth in current clamp mode. Our noise floor is nearly three times lower, at 8.2 μVrms across 10 kHz as measured in current clamp mode over 100 ms (Fig. 3D).

To assess the effectiveness of the temperature calibration, we connected PatchChip to a 1.0 GΩ resistor and clamped the voltage across the resistor to 100 mV, producing a 100 pA set current. The output of the voltage clamp current measurement circuitry was recorded along with the on-chip temperature sensor reading while the chip underwent a change in temperature from 3.5°C to 24.5°C. When left uncorrected, the current measurements are strongly dependent on temperature (Fig. 4A); however, this relationship is accurately fit (Pearson's r, $r = 0.99$, $p < 0.01$) using a second-order polynomial. Using this function to correct for temperature yields current measurements that are accurate to ±3% across this 21°C temperature range; we expect this relationship to continue for higher temperatures, such as typical body temperatures, as well. Long-term drift and stability of the voltage clamp circuit was measured across two hours in a constant-temperature environment. The current measurements were found to stay within ±3% of the true value over this period of time (Fig. 4B).

In Vitro Testing

The PatchChip headstage was mounted on a motorized manipulator (Sutter Instrument Company, Novato, CA) and integrated with a standard inverted microscope for *in vitro* patch-clamping experiments (Fig. 5A). We first performed voltage clamp and current clamp experiments on cultured HEK293FT cells. The PatchChip was set to voltage clamp mode and the resistance of the pipette was monitored in real time using the interface software in order to determine when the electrode tip had contacted a cell and a gigaseal (a tight electrical and mechanical seal with > 1 GΩ of resistance to the extracellular fluid) had formed. After obtaining a gigaseal,

either a short suction pulse or a high-amplitude voltage pulse (1 V, 1.0 ms) from the PatchChip was used to break the cell membrane at the electrode contact point to attain a whole-cell configuration. Representative currents measured from a voltage clamped HEK293FT cell are comparable to those measured using standard commercially available patch-clamp amplifiers (Fig. 5B).

In a similar fashion, we performed whole-cell patch-clamp measurements on cultured neurons (Fig. 5C). Representative traces of membrane potential voltages from a whole-cell patch-clamped neuron (access resistance, Ra = 22 MΩ; membrane resistance, Rm = 274 MΩ; membrane time constant, τ = 12.8 ms; membrane capacitance, Cm = 46.7 pF) were measured in current clamp mode in response to injected currents ranging from -100 pA to +150 pA (Fig. 5D). Current injection above 75 pA resulted in the cells being depolarized above threshold leading to action potential firing. In an extended current clamp experiment, the spontaneous membrane potential changes were recorded while a constant current (I = -30 pA) was injected (Fig. 5E). The cell fired action potentials at a rate of roughly 10 Hz, a physiologically realistic firing rate. Fig. 5F shows a representative current trace from the same neuron when it was voltage clamped near its resting potential of -70 mV. Miniature post-synaptic currents (mPSCs) of average peak amplitude of 23±11.8 pA (mean ± standard error; n = 7), and mean decay time 4.8±1.8 ms (mean ± standard error, n = 7) are observed at time points indicated by the dots plotted along the time axes (Fig. 5F). These results demonstrate the ability of the PatchChip to perform millisecond time resolution measurements of subthreshold synaptic events, as well as supra-threshold spiking events from single neurons *in vitro* and can thus be used for a wide range of electrophysiological characterizations of excitable cells.

A limitation in the current implementation of the PatchChip is the cross-over distortion that occurs when the measured current changes direction during voltage clamp. When current changes direction, the output of the op amp (Fig. 2A, B) cannot switch instantaneously between the two feedback diodes (M1 and M2 in Fig. 2B). This creates a “kink” in the current measurement (duration = 1.4 ms), causing the response to deviate from the expected first-order exponential (Fig 5G).

In Vivo Testing

The PatchChip was integrated with the “autopatcher” – a robotic system that automatically performs in vivo patch-clamping as demonstrated previously using commercially available amplifiers (Kodandaramaiah et al., 2012). We modified our existing software to incorporate autopatcher modules that allowed automated control of motor movement and pipette pressure. The PatchChip served as a custom headstage on an existing autopatcher setup (Fig. 6A). In one trial, upon the initiation of the autopatcher algorithm, a neuron was found at a depth of 452 μm in the brain. A multi-gigaohm seal was achieved in approximately 90 seconds (Fig. 6B). A whole-cell configuration was achieved by “zapping”, using a 1V, 50 μs pulse for break-in. We performed both voltage clamp and current clamp measurements on the neuron (access resistance, Ra = 72 MΩ; membrane resistance, Rm = 120 MΩ; membrane time constant, τ = 27.4 ms; membrane capacitance, Cm = 228 pF; Fig. 6B (inset), C), observing action potentials when currents of 200 pA or more were injected into the cell.

Discussion

We have designed and fabricated the ‘PatchChip’ for patch-clamp electrophysiology using standard silicon fabrication processes and have tested it in HEK293FT cells, cultured neurons, and in an in-vivo mouse preparation. In these settings, the PatchChip performed whole-cell patch-clamp measurements in both current and voltage clamp modes which enabled detection of millisecond-timescale sub-threshold events and supra-threshold action potential firing events from single neurons. These results demonstrate the versatility of the PatchChip in a variety of experimental settings.

The performance of the chip presented in this paper is currently limited by cross-over distortion and low series resistance compensation capability. The cross-over distortion creates an artifact in the recording that alters current measurements that are near zero. Improvements to the bandwidth and slew rate of the op amp should reduce this effect. The PatchChip is also limited by its range of series resistance compensation which goes up to 32 MΩ, though this can also be extended in future revisions. This is primarily a limitation for in-vivo whole-cell recordings in aged animals where series resistance can reach over 100 MΩ (Margrie et al., 2002), and to a lesser extent, for dendritic recordings (Stuart et al., 1993). On the other hand, when performing whole-cell somatic recordings in neuronal cultures (Hamill et al., 1981) and brain slices (Stuart et al., 1993), access

330 resistance is typically less than 30 MΩ which is within the range of series resistance compensation of the
331 PatchChip.

332

333 The realization of an on-chip patch amplifier using standard silicon fabrication processes will dramatically drive
334 down the cost and physical scale of patch-clamping instrumentation. Combining the PatchChip with recent
335 advances in automation of the patch-clamp technique will greatly expand the market for patch-clamp
336 instrumentation in both academia and industry. In particular, applications where a large number of
337 simultaneous intracellular recordings is required continue to multiply as researchers aim to record intracellular
338 signals from more and more neurons (Perin and Markram, 2013). The availability of affordable, automated,
339 multi-channel patch-clamp instrumentation represents an innovative technology that has the potential to
340 energize an already productive research area in neuroscience and medicine (Kodandaramaiah et al., 2013).
341 Automated patch clamping has even recently been used in conjunction with optogenetic neural control,
342 potentially enabling new ways of synapse-level circuit analysis (Chuong et al., 2014).

343 The PatchChip presented in this paper will be refined and optimized, and multiple patch-clamp amplifiers will
344 be fabricated on a single chip to serve emerging instrumentation requirements of highly scalable multi-channel
345 patch-clamp recording. In addition to scalability, this integrated electronic amplifier represents an enabling
346 technology for bench-top commoditized patch-clamping systems.

347

348 **Acknowledgements**

349 RRH acknowledges funding by the NIH 1R43NS083108-01. AAC, MFB and ESB acknowledge funding by The
350 Simons Center for the Social Brain (SCSB). ESB acknowledges funding by NIH 1R01EY023173, NIH
351 1R01MH103910-01, the New York Stem Cell Foundation-Robertson Award, NSF CBET 1053233, and the IET
352 Harvey Prize. IK and CRF acknowledge the NIH Computational Neuroscience Training Grant (DA032466-02).
353 CRF acknowledges the NIH BRAIN Initiative Grant (NEI and NIMH 1-U01-MH106027-01), the NIH Single Cell
354 Grant 1 R01 EY023173, NSF (EHR 0965945 and CISE 1110947), Georgia Tech Translational Research
355 Institute for Biomedical Engineering & Science (TRIBES) Seed Grant Awards Program, Georgia Tech Fund for
356 Innovation in Research and Education (GT-FIRE),Wallace H. Coulter Translational/Clinical Research Grant

Program and support from Georgia Tech through the Institute for Bioengineering and Biosciences Junior Faculty Award, Technology Fee Fund, Invention Studio, and the George W. Woodruff School of Mechanical Engineering.

Competing Financial Interests

RRH is a co-founder of Intan and maintains equity in this company.

References

Chen WS, Bear MF. Activity-dependent regulation of NR2B translation contributes to metaplasticity in mouse visual cortex. *Neuropharmacology* 52: 200–214, 2007.

Chuong AS, Miri ML, Busskamp V, Matthews GAC, Acker LC, Sørensen AT, Young A, Klapoetke NC, Henninger MA, Kodandaramaiah SB, Ogawa M, Ramanlal SB, Bandler RC, Allen BD, Forest CR, Chow BY, Han X, Lin Y, Tye KM, Roska B, Cardin JA, Boyden ES. Noninvasive optical inhibition with a red-shifted microbial rhodopsin. *Nat Neurosci* 17: 1123–1129, 2014.

Goldstein B, Choe K, Sigworth FJ, Culurciello E. A four-channel integrated patch-clamp amplifier with current-clamp capability. 2011 IEEE 54th International Midwest Symposium on Circuits and Systems (MWSCAS). 2011, p. 1 –4.

Hamill OP, Marty A, Neher E, Sakmann B, Sigworth FJ. Improved patch-clamp techniques for high-resolution current recording from cells and cell-free membrane patches. *Pflüg Arch* 391: 85–100, 1981.

Harrison RR, Charles C. A low-power low-noise CMOS amplifier for neural recording applications. *IEEE J Solid-State Circuits* 38: 958–965, 2003.

Hodgkin AL, Huxley AF. A quantitative description of membrane current and its application to conduction and excitation in nerve. *J Physiol* 117: 500–544, 1952.

Klapoetke NC, Murata Y, Kim SS, Pulver SR, Birdsey-Benson A, Cho YK, Morimoto TK, Chuong AS, Carpenter EJ, Tian Z, Wang J, Xie Y, Yan Z, Zhang Y, Chow BY, Surek B, Melkonian M, Jayaraman V, Constantine-Paton M, Wong GK-S, Boyden ES. Independent optical excitation of distinct neural populations. *Nat Methods* 11: 338–346, 2014.

Kodandaramaiah SB, Boyden ES, Forest CR. In vivo robotics: the automation of neuroscience and other intact-system biological fields. *Ann N Y Acad Sci* 1305: 63–71, 2013.

Kodandaramaiah SB, Franzesi GT, Chow BY, Boyden ES, Forest CR. Automated whole-cell patch-clamp electrophysiology of neurons in vivo. *Nat Methods* 9: 585–587, 2012.

Laiwalla F, Klemic KG, Sigworth FJ, Culurciello E. An Integrated Patch-Clamp Amplifier in Silicon-on-Sapphire CMOS. *IEEE Trans Circuits Syst Regul Pap* 53: 2364 –2370, 2006.

Margrie TW, Brecht M, Sakmann B. In vivo, low-resistance, whole-cell recordings from neurons in the anaesthetized and awake mammalian brain. *Pflüg Arch* 444: 491–498, 2002.

Mead C. *Analog VLSI and Neural Systems*. Boston, MA, USA: Addison-Wesley Longman Publishing Co., Inc., 1989.

Molecular Devices. Axon Axoclamp 900A Microelectrode Amplifier [Online]. date unknown. http://www.moleculardevices.com/Products/Instruments/Axon-Patch-Clamp/Axon-Axoclamp.html [23 Jun. 2014a].

Molecular Devices. Axon Axopatch 200B Capacitor Feedback Patch Clamp Amplifier [Online]. date unknown. http://www.moleculardevices.com/Products/Instruments/Axon-Patch-Clamp/Axon-Axopatch.html [23 Jun. 2014b].

Molleman A. Whole-Cell Protocols and Data Analysis [Online]. In: *Patch Clamping*. John Wiley & Sons, Ltd, p. 115–139. http://onlinelibrary.wiley.com/doi/10.1002/0470856521.ch5/summary [23 Jun. 2014].

Neher E, Sakmann B. Single-channel currents recorded from membrane of denervated frog muscle fibres. *Nature* 260: 799–802, 1976.

Pantoja R, Nagarah JM, Starace DM, Melosh NA, Blunck R, Bezanilla F, Heath JR. Silicon chip-based patch-clamp electrodes integrated with PDMS microfluidics. *Biosens Bioelectron* 20: 509–517, 2004.

Perin R, Markram H. A Computer-assisted Multi-electrode Patch-clamp System. *J Vis Exp* , 2013.

Safronov BV, Vogel W. Electrical Activity of Individual Neurons: Patch-Clamp Techniques [Online]. In: *Modern Techniques in Neuroscience Research*, edited by Windhorst PDU, Johansson PDH. Springer Berlin Heidelberg, p. 173–192. http://link.springer.com/chapter/10.1007/978-3-642-58552-4_6 [23 Jun. 2014].

Sakmann B, Neher E. *Single-channel recording*. 2nd ed. New York, NY: Springer New York, 2009.

Sigworth FJ. Design of the EPC-9, a computer-controlled patch-clamp amplifier. 1. Hardware. *J Neurosci Methods* 56: 195–202, 1995.

Stuart GJ, Dodt HU, Sakmann B. Patch-clamp recordings from the soma and dendrites of neurons in brain slices using infrared video microscopy. *Pflüg Arch* 423: 511–518, 1993.

Tuthill M. A switched-current, switched-capacitor temperature sensor in 0.6- mu;m CMOS. *IEEE J Solid-State Circuits* 33: 1117–1122, 1998.

Vittoz E, Fellrath J. CMOS analog integrated circuits based on weak inversion operations. *IEEE J Solid-State Circuits* 12: 224–231, 1977.

Weerakoon P, Culurciello E, Yang Y, Santos-Sacchi J, Kindlmann PJ, Sigworth FJ. Patch-clamp amplifiers on a chip. *J Neurosci Methods* 192: 187–192, 2010.

Table 1: Electrical characteristics of existing patch-clamp amplifiers

Parameter	**Axopatch 200B or Axoclamp 900A**(Molecular Devices)	Weerakoon et al., 2010 **and** Goldstein et al., 2011	**PatchChip**
Noise floor for current measurements (voltage clamp)	0.65 pA rms over 5 kHz (high gain) 1.65 pA rms over 5 kHz (low gain)	8 pA rms over 10 kHz	1.1 pA rms over 5 kHz
Noise floor for voltage measurements (current clamp)	23 μV rms over 10 kHz	150 μV rms over 5 kHz	8.2 μV rms over 10 kHz
Series resistance compensation	0 – 100 MΩ	0 – 80 MΩ	0 – 32 MΩ
Capacitance compensation	0 – 10 pF	0 – 10 pF	0 – 10 pF

Figure 1: A simplified schematic of a traditional patch-clamp amplifier in voltage clamp mode. A FET-input op-amp uses feedback to hold the pipette voltage V_P at the user-specified potential V_{clamp}. The whole-cell current I_{cell} passes through feedback resistor R_{Fn} selected by switch S_1. The resulting output voltage is linearly proportional to the measured current. Several different feedback resistors are needed to accurately measure different current ranges from picoamps to nanoamps. These resistors must be in the high MΩ and GΩ range, making them relatively large and impractical to integrate on a chip.

Figure 2: **A.** Simplified schematic of the voltage clamp circuitry in PatchChip. On-chip diodes are used in place of large-valued feedback resistors. Diodes have an exponential relationship between voltage and current, as well as a sensitivity to temperature. Depending on the direction of I_{cell} either D_1 or D_2 will conduct; and the output voltage will be a logarithmic function of the measured current. An on-chip temperature sensor can be used to factor out temperature dependencies. **B.** Detailed schematic of voltage clamp circuit showing transistors M1-M6 that implement the diode-like feedback elements.

Figure 3: PatchChip design and benchtop characteristics **A.** Microphotograph of the PatchChip. Each silicon chip measures 4.7 mm × 3.0 mm and contains more than 20,000 transistors, resistors, and capacitors. **B.** Circuit board containing the PatchChip (in black plastic leaded chip carrier (PLCC) package labeled "Intan") and supporting components. The aluminum enclosure (measuring 8.5 cm × 5.7 cm × 2.9 cm) shields the sensitive electronics from interference. This circuit board contains the functionality of the head stage as well as the rack-mounted amplifier and analog-to-digital converter in traditional patch-clamp amplifier systems. All current and voltage measurements are digitized on this circuit board and passed to a USB interface board over digital serial cables. **C.** Measured voltage noise floor of PatchChip in current clamp (injected I = 0) mode. Noise over the 10 kHz bandwidth was 8.2 μV rms. **D.** Measured current noise floor of PatchChip in voltage clamp mode measuring 100 pA current. Noise over the 5 kHz bandwidth was 1.1 pA rms.

Figure 4: Temperature-dependent and time-dependent voltage clamp measurements. A 1 GΩ resistor was voltage clamped at 100 mV, producing a set current of 100 pA (dashed) **A.** Correction of temperature-dependent voltage clamp measurements. The uncorrected current measurements (square) vary predictably with temperature. A second-order polynomial (solid) is used to correct the measurements based on the reading from the on-chip temperature sensor. The corrected measurements (circle) lie within +/-3% of the true current over a temperature change of 21°C. **B.** Time drift of voltage clamp measurements. Over a period of 120 minutes, the measured current deviates by less than ±3% (circle) from the set current (dashed).

Figure 5: In-vitro PatchChip performance **A.** PatchChip (inside aluminum box with blue interface cables) with glass pipette electrode connected. The blue cables convey power and digital data between the PatchChip circuitry and a host computer. The dish contains cultured HEK293FT cells. The PatchChip module is attached to a three-axis micropositioner that allows the electrode tip to precisely contact a cell. **B.** HEK293FT voltage clamp experiments using the PatchChip. Ionic currents in whole-cell mode (top) in response to different command voltages (bottom). Current levels and time constants are consistent with typical HEK293FT cell characteristics. **C.** Microscope view showing the tip of glass pipette contacting a cultured neuron. The pipette was connected to the PatchChip, and voltage clamp and current clamp experiments were performed on the cell. Scale bar: 10 µm **D.** Current clamp experiment using the PatchChip. Action potentials are evoked when the injected current exceeds 75 pA. **E.** In vitro current clamp recordings from cultured neurons using the PatchChip. A clamping current of -30 pA is being injected into the cell. Spontaneous action potentials firing at a physiological rate are visible in the measured voltage waveform. **F.** Voltage clamp experiment using the PatchChip. The cell is being held near its resting potential of -70 mV. Miniature post-synaptic currents (mPSCs) in the picoamp range from spontaneous activity are visible (*****). **G.** Crossover distortion in the voltage-clamp circuit when measured current switches direction. Passive membrane characteristics of a neuron were measured by using sodium channel blockers and stepping the control voltage from -70 mV to -40 mV. Arrow indicates a "kink" artifact lasting approximately 1.4 ms that occurs due to crossover distortion. The ideal passive response of a cell to this voltage step is a first-order exponential (dashed).

Figure 6: In-vivo PatchChip performance **A.** The PatchChip (inside aluminum box with blue power/data cables) connected to the "autopatcher", an automated in-vivo patch-clamping robot. **B.** Pipette electrode resistance measured by the PatchChip during a 100-second in vivo "autopatcher" experiment in which a seal of >3 GΩ was achieved using an automated robotic system incorporating the PatchChip. Successful membrane break-in to achieve whole cell configurations occurred at t = 97 seconds. Current traces recorded in voltage clamp in response to +5 mV, 10 Hz square wave pulses ($V_{holding}$ = -72 mV) show RC transients typical of a whole-cell patch-clamped cell **(inset) C.** *In vivo* neuron current clamp measurements taken with the PatchChip and autopatcher system from the neuron shown in **B**. Action potentials were visible when the injected current exceeded 100 pA.

Table 1: Electrical characteristics of existing patch-clamp amplifiers

Parameter	**Axopatch 200B or Axoclamp 900A**(Molecular Devices)	Weerakoon et al., 2010 **and** Goldstein et al., 2011	**PatchChip**
Noise floor for current measurements (voltage clamp)	0.65 pA rms over 5 kHz (high gain) 1.65 pA rms over 5 kHz (low gain)	8 pA rms over 10 kHz	1.1 pA rms over 5 kHz
Noise floor for voltage measurements (current clamp)	23 μV rms over 10 kHz	150 μV rms over 5 kHz	8.2 μV rms over 10 kHz
Series resistance compensation	0 – 100 MΩ	0 – 80 MΩ	0 – 32 MΩ
Capacitance compensation	0 – 10 pF	0 – 10 pF	0 – 10 pF

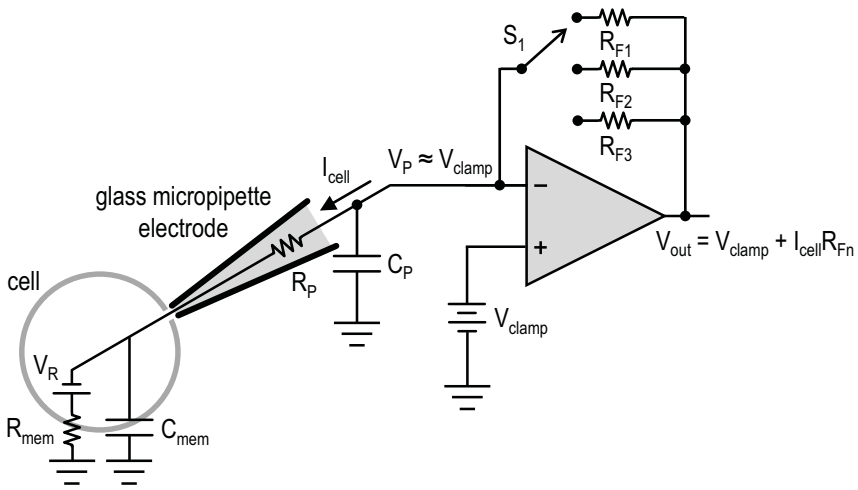
S1
RF1
RF2
RF3
Icell
VP ≈ Vclamp
glass micropipette
electrode
cell
CP
RP
Vout = Vclamp + IcellRFn
Vclamp
VR
Rmem
Cmem

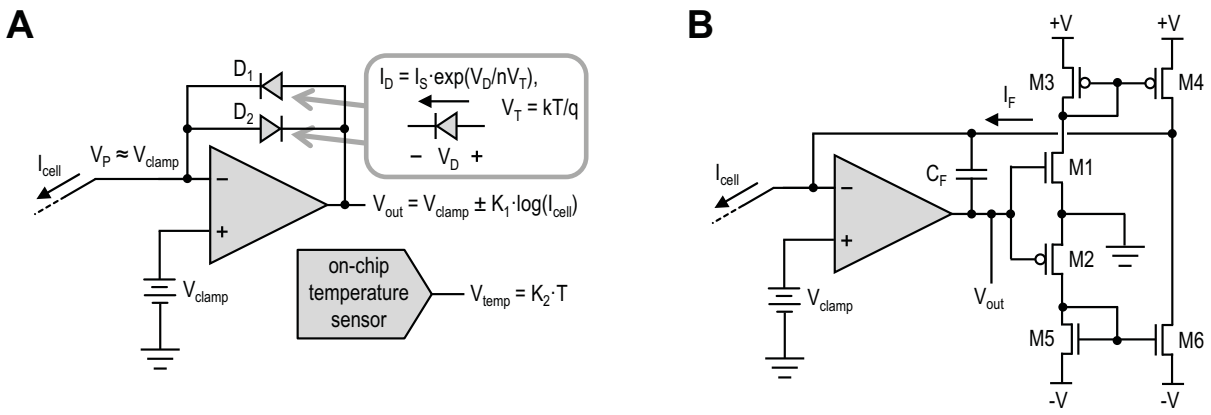
A
D1
D2
ID = IS·exp(VD/nVT),
VT = kT/q
– VD +
Icell
VP ≈ Vclamp
Vout = Vclamp ± K1·log(Icell)
Vclamp
on-chip
temperature
sensor
Vtemp = K2·T
B
+V
+V
M3
M4
IF
Icell
CF
M1
M2
Vclamp
Vout
M5
M6
-V
-V

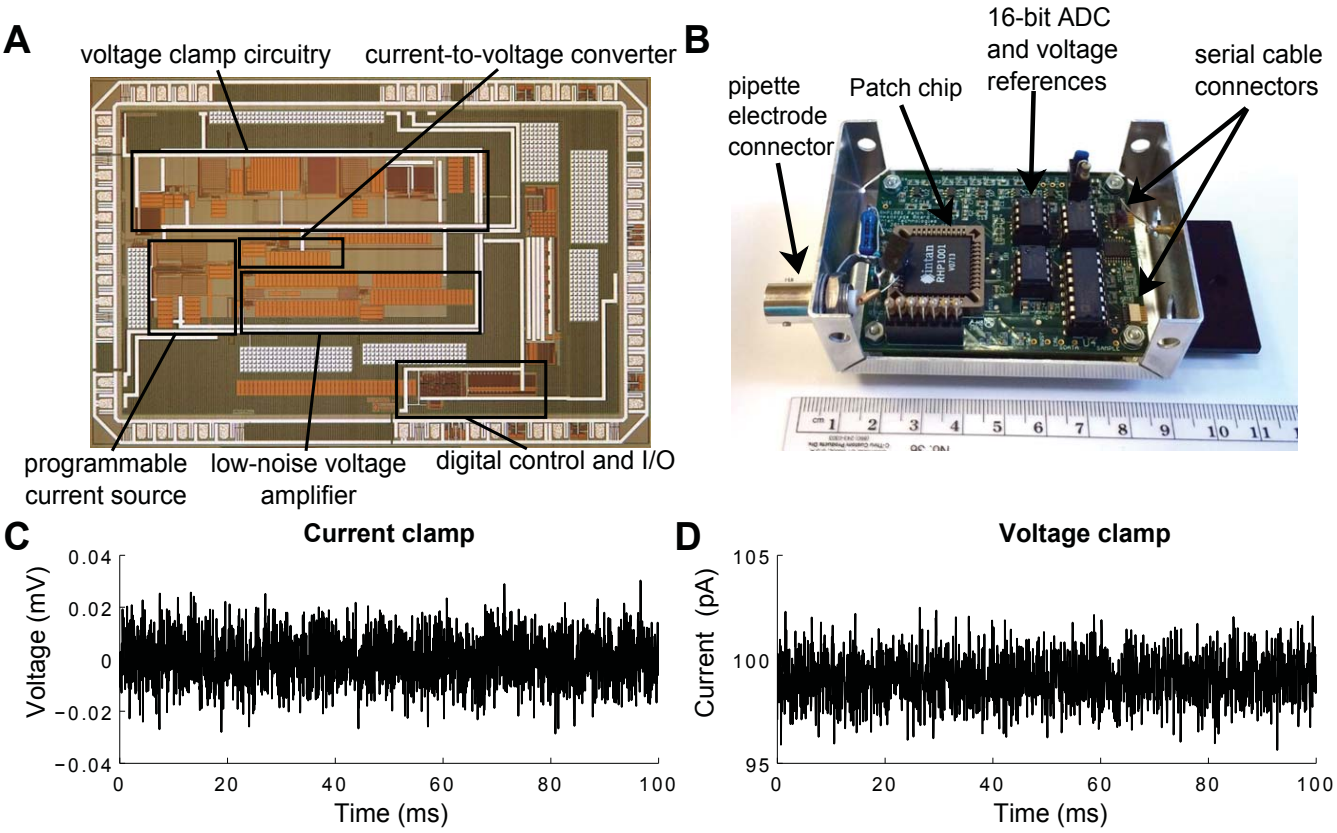
A
voltage clamp circuitry
current-to-voltage converter
programmable current source
low-noise voltage amplifier
digital control and I/O
B
16-bit ADC and voltage references
serial cable connectors
pipette electrode connector
Patch chip
C
Current clamp
Voltage (mV)
0.04
0.02
0
−0.02
−0.04
0
20
40
60
80
100
Time (ms)
D
Voltage clamp
Current (pA)
105
100
95
0
20
40
60
80
100
Time (ms)

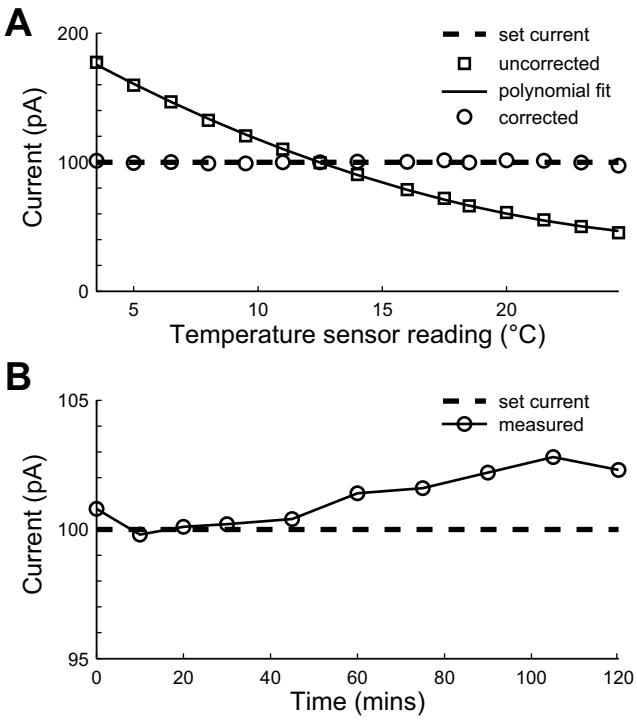
A
200
100
0
Current (pA)
5
10
15
20
Temperature sensor reading (°C)
set current
uncorrected
polynomial fit
corrected
B
105
100
95
Current (pA)
0
20
40
60
80
100
120
Time (mins)
set current
measured

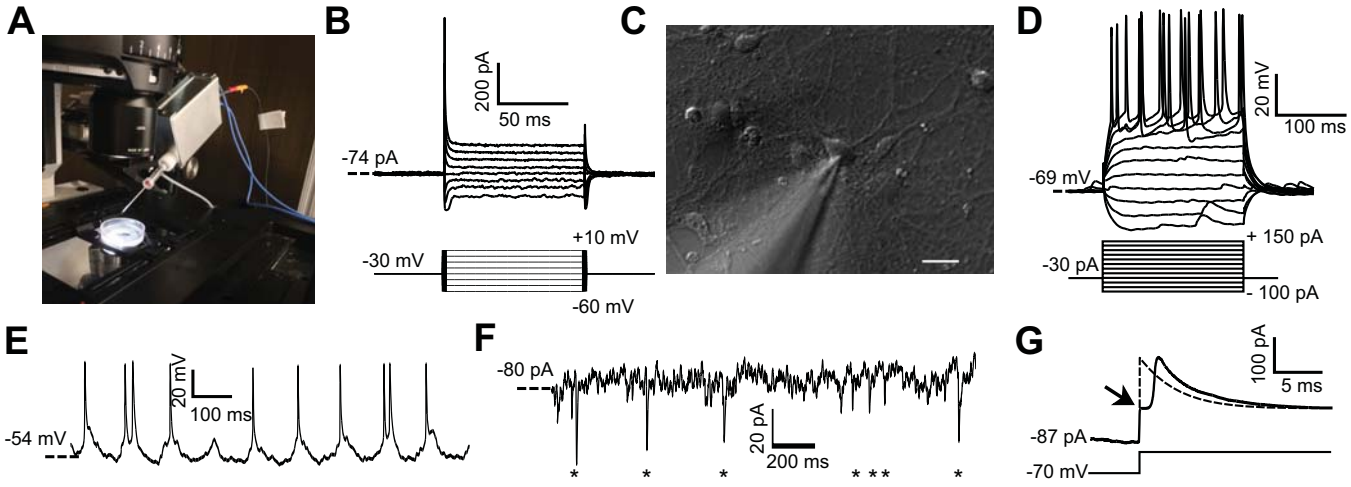
A
B
C
D
200 pA
50 ms
-74 pA
+10 mV
-30 mV
-60 mV
20 mV
100 ms
-69 mV
+ 150 pA
-30 pA
- 100 pA
E
20 mV
100 ms
-54 mV
F
-80 pA
20 pA
200 ms
G
100 pA
5 ms
-87 pA
-70 mV

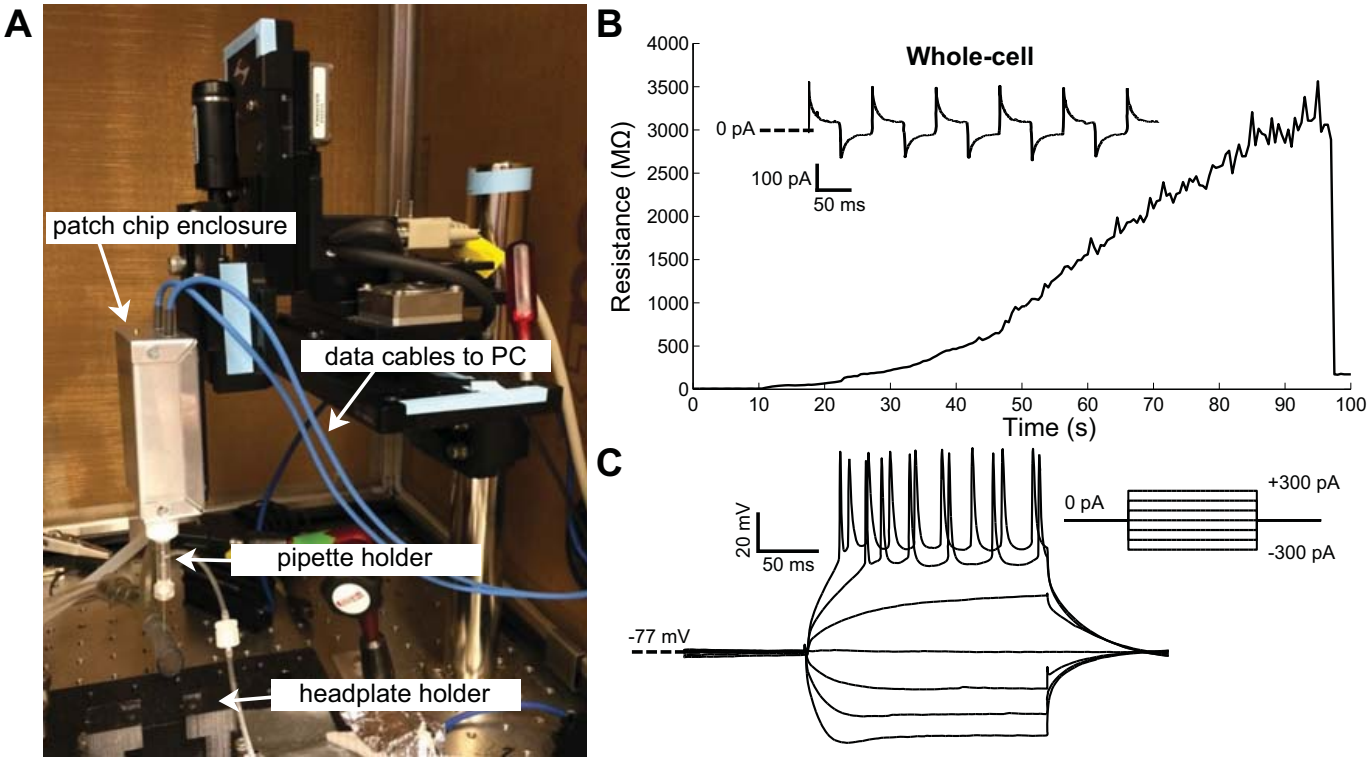
A
patch chip enclosure
data cables to PC
pipette holder
headplate holder
B
Whole-cell
Resistance (MΩ)
Time (s)
0 pA
100 pA
50 ms
C
20 mV
50 ms
0 pA
+300 pA
-300 pA
-77 mV